Science Bulletin 68 (2023) 674–678

Contents lists available at ScienceDirect

Science Bulletin

journal homepage: www.elsevier.com/locate/scib

Short Communication

Emergence of superconducting dome in ZrN_x films via variation of nitrogen concentration

Fucong Chen [a,b], Xinbo Bai [a,b], Yuxin Wang [a], Tao Dong [c], Jinan Shi [b], Yanmin Zhang [a], Xiaomin Sun [d], Zhongxu Wei [a], Mingyang Qin [a], Jie Yuan [a,e], Qihong Chen [a,e], Xinbo Wang [a], Xu Wang [a], Beiyi Zhu [a], Rongjin Huang [d], Kun Jiang [a], Wu Zhou [b], Nanlin Wang [c], Jiangping Hu [a], Yangmu Li [a,b,*], Kui Jin [a,e,*], Zhongxian Zhao [a,e]

[a] Beijing National Laboratory for Condensed Matter Physics, Institute of Physics, Chinese Academy of Sciences, Beijing 100190, China
[b] School of Physical Sciences, University of Chinese Academy of Sciences, Beijing 100049, China
[c] International Center for Quantum Materials, School of Physics, Peking University, Beijing 100871, China
[d] CAS Key Laboratory of Cryogenics, Technical Institute of Physics and Chemistry, Beijing 100190, China
[e] Songshan Lake Materials Laboratory, Dongguan 523808, China

ARTICLE INFO

Article history:
Received 14 February 2023
Received in revised form 8 March 2023
Accepted 9 March 2023
Available online 13 March 2023

Most superconductors can be categorized into two classes – the conventional Bardeen-Cooper-Schrieffer (BCS) superconductors [1] and the unconventional superconductors including the strongly correlated high-T_c superconductors [2]. For typical high-T_c superconductors, their parent compounds are Mott or charge transfer insulators. Upon chemical substitutions, a superconducting dome emerges close to the strongly insulating phase. The recent realization of strongly insulating states and superconducting dome in the twisted multi-layer graphene [3] and van der Waals materials [4] suggests that certain features of unconventional superconductivity may not be limited to 3*d* transition metal compounds such as Cu- [2], Fe- [5], and Ni-based superconductors [6]. In this work, we present a compelling case that seemingly unconventional superconducting and normal-state properties can result from conventional mechanisms such as disorder and electron–phonon coupling.

The nature of superconductivity in transition metal nitrides has not been settled since their discovery [7]. Although their superconducting properties, including superconducting gaps and upper critical fields, can be explained by the BCS physics, a few early works also reported experimental observations that require theory beyond the BCS picture, e.g., the density of states at the Fermi surface [8] and electron–phonon coupling strength [9] are too low to account for their relatively high T_c. Meanwhile, because of their mechanical hardness and durability, superconducting transition metal nitrides have attracted a lot of attention lately for their unique advantages in technological applications.

ZrN has a NaCl structure with lattice constants of ~4.60 Å, which belongs to the $Fm\bar{3}m$ space group and the O_h point group. ZrN_x studied previously often has multiple structure domains. Here, we grew (00*l*) oriented ZrN_x films on (00*l*) MgO substrate with thicknesses of ~150 nm using the pulsed laser deposition. By employing fine controls of nitrogen partial pressure and the relative position between the substrate and target, ZrN_x films with x from 0.54 to 1.40 were obtained. The N concentration and crystal lattice parameters were measured with the energy dispersive X-ray spectroscopy (EDX, Fig. S1 online) and X-ray diffraction (XRD, Fig. S2 online). All ZrN_x thin films studied in this work have the same ZrN $Fm\bar{3}m$ structure (Table S1 online).

Fig. 1 illustrates the temperature-dependent resistivity of ZrN_x films. For $x \sim 1.00$, the onset superconducting transition temperature, T_c^{onset}, reaches a maximum value of 10 K, consistent with that of the bulk ZrN_x [7]. For the *N*-rich region ($x > 1.00$), T_c^{onset} gradually decreases towards zero and a strongly insulating phase develops. The resistivity rises by two orders of magnitude from 300 to 2 K (Fig. 1a), and a resistivity upturn appears (Fig. 1b). Notably, the onset superconducting transition is clearly seen for insulating ZrN_x with $1.30 \leq x \leq 1.35$. For the *N*-deficient region ($x < 1.00$), a decrease of T_c^{onset} coincides with the presence of a weakly insulating phase, for which the resistivity upturn is much less obvious (Fig. 1b). Representative temperature-dependent magnetic susceptibility of ZrN_x is delineated in Fig. 1c. The superconducting volume

* Corresponding authors.
E-mail addresses: yangmuli@iphy.ac.cn (Y. Li), kuijin@iphy.ac.cn (K. Jin).

https://doi.org/10.1016/j.scib.2023.03.018
2095-9273/

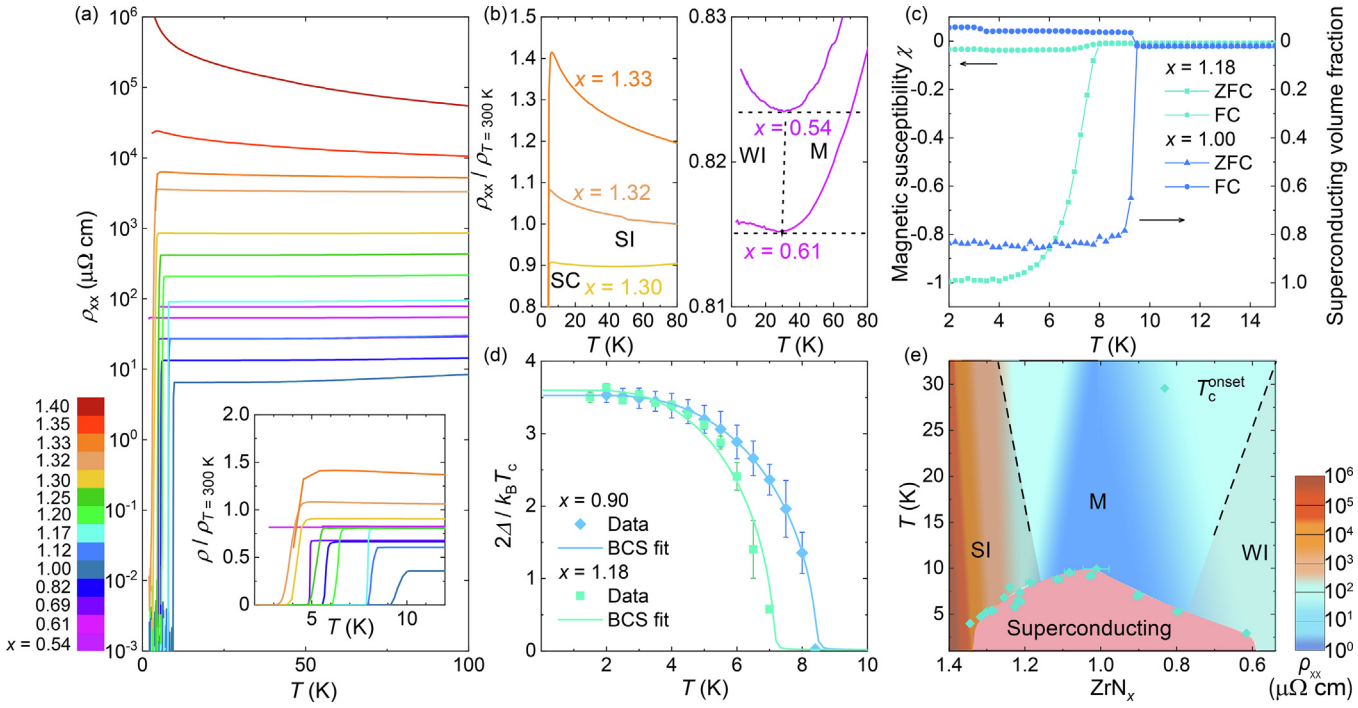

Fig. 1. (Color online) (a) Temperature-dependent resistivity of ZrN_x with various x. (b) Resistivity upturns in the N-rich (left panel) and N-deficient (right panel) regions. SC, SI, WI, and M correspond to the superconducting, strongly insulating, weak insulating, and metallic phases, respectively. (c) Representative magnetic susceptibility and superconducting volume fraction. (d) Temperature dependence of superconducting gap, 2Δ, measured by Terahertz spectroscopy. (e) Phase diagram of ZrN_x. The color shades outside of the superconducting dome indicate the magnitude of electrical resistivity. The two dashed lines labeling the phase boundaries are determined by the temperature derivative of the resistivity that equals zero.

fraction is found to be close to 1, suggesting bulk rather than surface superconductivity. We performed measurement of the superconducting energy gap, 2Δ, using Terahertz spectroscopy (see Terahertz raw data in Fig. S3 online). As plotted in Fig. 1d, the temperature dependence of 2Δ can be well explained by the BCS gap function, $2\Delta/k_BT_c \sim (1-\frac{T}{T_c})^{1/2}$ [1]. In Fig. 1e, we construct a phase diagram for ZrN_x. Strikingly, the superconducting dome emerges in the close vicinity of a strongly insulating (SI) phase and a metallic (M) state exists above T_c near the optimal N concentration.

The electrical transport properties of normal state ZrN_x have been analyzed quantitatively (see Figs. S4 and S5 (online) for full results). A normal state phase diagram has been summarized, as in Fig. 2a. Interestingly, the longitudinal resistivity, ρ_{xx}, can be described by linear-in-temperature and quadratic-in-temperature regimes above superconducting dome. This resistivity behavior, $\rho_{xx} = \rho_0 + A_1T + A_2T^2$, where A_1 and A_2 are resistivity prefactors and ρ_0 is the residual resistivity, imitates resistivity in the normal-state of unconventional superconductors [10,11] Hall coefficient R_H is plotted in Fig. 2b, which is insensitive to the temperature, indicating a relatively simple Fermi surface. To further investigate the underlying physics, In Fig. S6 (online), we carried out the additional analyses of ρ_{xx}, using Matthiessen rule with electron–phonon scattering. This method describes our resistivity data very well. In Fig. S7 (online), we calculated the band structure and Fermi surface for ZrN_x using density-functional theory (DFT), employing the projector augmented wave method and the generalized gradient approximation. We observe the existence of electron Fermi pockets, which are consistent with the negative sign of the Hall resistivity. Raman spectroscopy has been carried out to characterize the ZrN_x phonon modes at room temperature. Theoretically, due to the O_h point symmetry of the ZrN structure, the first-order Raman scattering should be prohibited. However, the excess/absent N atoms and disorders can destroy the symmetry protection, leading to the rise of acoustic and optical phonon Raman intensities [12]. Fig. 2c illustrates the Raman spectra of ZrN_x with various x (detailed Raman data in Fig. S8 online). We convert the Raman shift of acoustic phonon modes to the electron–phonon coupling constant $\lambda \propto 1/\omega^2$ in Fig. 2d [12], which reveals a significant weakening of λ in the N-deficient region. Because both Raman intensities and residual resistivity ρ_0 can reflect the amount of disorders in ZrN_x, we compare them in Fig. 2e, which display a large enhancement in the SI phase.

To further investigate the disorder in the SI phase, we performed scanning transmission electron microscopy (STEM) measurements on ZrN_x with $x = 1.00$, 1.25, 1.35. STEM data at the atomic scale for $x = 1.25$ reveal additional N atoms located between the Zr atoms (also see Fig. S7 online for STEM data with other x). We summarize the evolution of the superconducting dome in Fig. 2f. At $x = 1.00$, ZrN_x has an optimal T_c of 10 K. With a lowering x, the electron–phonon coupling obtained from Raman scattering decreases. Applying McMillan's formula, we estimate the upper bound of the superconducting transition temperature, $T_c^* = (\theta_D/1.45)\exp[-\frac{1.04(1+\lambda)}{\lambda-\mu^*(1+0.62\lambda)}]$, where θ_D is the Debye temperature (~475 K from fit), μ^* is the Coulomb repulsion strength (~0.1 from fit). In the N-deficient region, the calculated T_c^* tracks the experimentally obtained T_c^{onset} very well. However, for the N-rich region, T_c^* is almost a constant, and thus cannot explain the lowering T_c^{onset}. Alternatively, assuming the presence of excess N atoms (Fig. 2g) can induce localization of otherwise mobile electrons due to bonding between negatively charged N and positively charged Zr atoms, we estimate the number of mobile electrons per Zr atoms, valence n_e/Zr, as a function of x in Fig. 2f (dashed line). The value of $n_e/\mathrm{Zr} \sim 4-3x$ for $x < 1.33$ reflects how many electrons can contribute to the normal state and superconductivity,

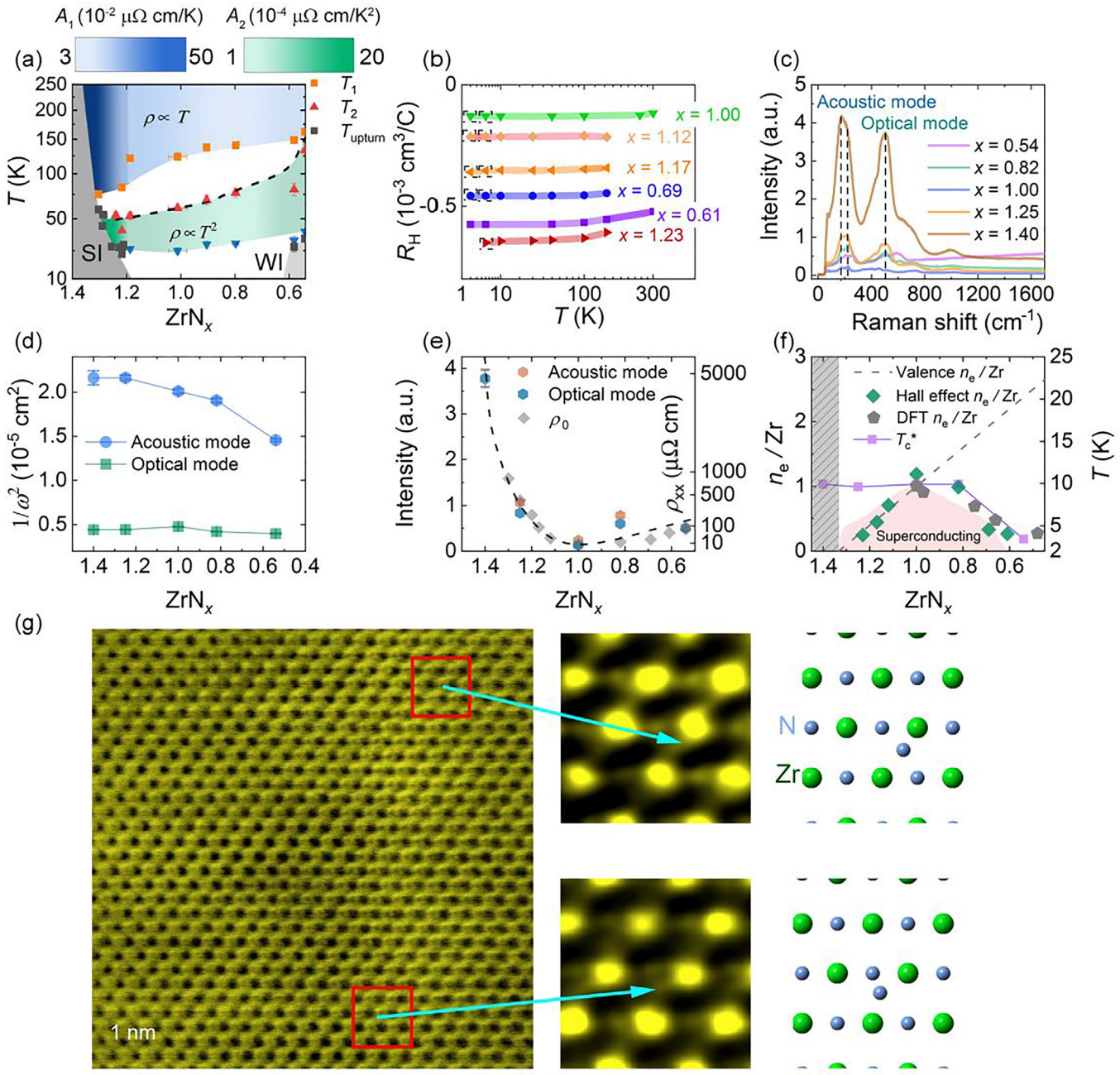

Fig. 2. (Color online) (a) Normal state phase diagram of ZrN_x based on electrical resistivity. (b) The Hall coefficient, R_H, as a function of N concentration and temperature. (c) Raman spectra of ZrN_x with various x. (d) Inverse square of the acoustic mode Raman shift, $1/\omega^2$, for acoustic and optical modes, which is proportional to the electron–phonon coupling. (e) Comparison between Raman scattering intensities and the residual resistivity, ρ_0. (f) Analysis for superconducting dome. Valence n_e/Zr and DFT n_e/Zr are number of estimated mobile electrons per Zr for *N*-rich and *N*-deficient regions, respectively. Hall effect n_e/Zr are the experimental data. Upper bound of the superconducting transition temperature, T_c^*, is calculated from $1/\omega^2$ based on the McMillan's formula. Dashed grey shade for $x > 1.33$ signifies an upper boundary for superconductivity. (g) STEM image of ZrN_x for $x = 1.25$. Additional N atoms (blue in the illustration) are revealed to locate between the Zr atoms (Green).

and it is found to be consistent with that extracted from Hall measurement for $x > 1.00$. We note that Zr_3N_4 was previously calculated to be a band insulator [13]. Our simple estimation here only based on the electron valency of Zr and N, with no requirement of using the Zr_3N_4 structure (all our ZrN_x films are characterized to be the ZrN $Fm\bar{3}m$ structure). In the *N*-deficient region, because the N to Zr ratio is less than one, our estimation based on excess N atoms no longer works. We performed DFT calculation with virtual crystal approximation. The DFT n_e/Zr is calculated by integrating density of states for Zr bands up to the energy where the integral of all bands equals to the number of carriers in the material. We compare the DFT calculated n_e/Zr to that extracted from Hall measurement and obtain a good correspondence for $x < 1.00$.

Our work thoroughly established the appearance of a superconducting dome near a strongly insulating phase in transition metal pnictides. This resemblance inevitably raises questions about the underlying physics of the superconducting dome in unconventional and seemingly conventional materials. For high-T_c superconductors, large onsite Coulomb repulsion results in Mott or charge transfer insulators that coexists with the long-range antiferromagnetism [3]. In the case of ZrN_x, our magnetic susceptibility mea-

surements observe no magnetic orderings inside and outside of the SI phase. STEM results (Fig. S9 online) demonstrate the appearance of interstitial N atoms when ZrN_x enters the SI phase, while no ordering of the interstitial N atoms has been observed. The drastic increase of resistivity and decrease in the number of carriers can thus be attributed to charge localization associated with additional N atoms. In principle, the reduction of mobile electrons would limit the number of Cooper pairs and lead to a lower T_c. In fact, based on the valency of Zr and N atoms, we estimate the upper superconducting dome boundary at $x = 1.33$, where $n_e/Zr \sim 4 - 3x = 0$. This estimation is consistent with experimental observed values in the *N*-rich region (Fig. 2f). The vanishing number of carriers in the normal state can result in a decreasing superfluid density in the superconducting state, similar to what happens in high-T_c superconductors, but its origin in conventional superconductors is yet to be explained. For the *N*-deficient region, T_c^{onset} is found to follow T_c^*, suggesting that the electron–phonon coupling dominates the evolution of the superconducting dome. This behavior differs from the case of high-T_c superconductors, where the superfluid density decreases in the over-doped regime while the number of carriers in the normal state increases [2].

Next, we compare the nature of the metallic normal state for ZrN_x to that in the other superconductor families. Although no consensual conclusion has been made on the underlying physics of the normal state for high-T_c superconductors, relevant main signatures include linear-in-temperature resistivity that goes above the Mott-Ioffe-Regel limit and a temperature-dependent Hall coefficient [2]. The scaling relation of resistivity prefactors was also linked to possible existence of quantum criticality and the emergence of superconductivity [14]. For ZrN_x, we only observe $\rho_{xx} \sim T$ resistivity near 250 K, almost half of the Debye temperature, while the resistivity magnitude is well below the Mott-Ioffe-Regel limit (Table S2 online). The $\rho_{xx} \sim T$ resistivity is thus more likely to associate with electron phonon scattering. The N concentration dependence of A_1, and A_2 also show no obvious scaling relation respective to x (Fig. 2a and Fig. S6 online), and they are closely related to ρ_0, that is suggestive of overall enhancement of resistivity instead of non-Fermi-liquid features. The nearly temperature-independent Hall coefficient, in addition, provides clear evidence for the persistence of a full Fermi surface, in contrast to that for high-T_c superconductors. Recently, the linear-in-temperature resistivity in high-T_c superconductors was found to be associated with the Planckian scattering rate, $\hbar/\tau \sim \alpha k_B T$, where α is close to 1 [15]. We estimate that the temperature range at which $\rho_{xx} \sim \propto A_1 T$ appears for ZrN_x is also much lower than the Planckian limit (Table S2 online). Thus, the resistivity of ZrN_x likely originates from an electron–phonon scattering of a Fermi-liquid normal state that relevant to excess and vacant N atoms.

ZrN_x presents a remarkable material system to study the emergence of a superconducting dome, for which an interplay between two distinct mechanisms can realize its evolution. Instead of requiring a temperature difference between electron pairing and phase coherence, tunable charge localization and pairing strength control the dome shape of superconductivity in ZrN_x. As an increasing number of studies observing superconducting domes in high-T_c superconductors [2,5,6] and two-dimensional materials, our discovery points to a new route in understanding the superconducting dome in these complex materials.

Conflict of interest

The authors declare that they have no conflict of interest.

Acknowledgments

We thank Lihong Yang, Hua Zhang, Xiaoli Dong, Huaixin Yang, and Zhanyi Zhao for assistant in experimental measurements and Jian Kang for useful discussions. This work was supported by the National Key Basic Research Program of China (2021YFA0718700, 2017YFA0302900, 2017YFA0303003, 2018YFB0704102, and 2018YFA0305800), the National Natural Science Foundation of China (11888101, 11927808, 11834016, 11961141008, 12174428, and 12274439), the Strategic Priority Research Program (B) of Chinese Academy of Sciences (XDB25000000, XDB33000000), CAS Interdisciplinary Innovation Team, Beijing Natural Science Foundation (Z190008), CAS through the Youth Innovation Promotion Association (2022YSBR-048), Key-Area Research and Development Program of Guangdong Province (2020B0101340002), and the Center for Materials Genome.

Author contributions

Kui Jin and Yangmu Li conceived and led the research with input from Zhongxian Zhao; Fucong Chen and Xinbo Bai synthesized the films; Fucong Chen, Xinbo Bai, and Xiaomin Sun carried out the electrical transport and magnetic susceptibility measurements with help from Jie Yuan, Qihong Chen, and Rongjin Huang; Tao Dong, Xinbo Wang, and Nanlin Wang performed Terahertz spectroscopy experiments; Yanmin Zhang obtained the Raman spectroscopy data; Jinan Shi and Wu Zhou carried out scanning transmission electron microscopy measurements; Fucong Chen analyzed the data with supports from Zhongxu Wei, Mingyang Qin, Xu Wang, and Beiyi Zhu; Yuxin Wang, Kun Jiang, and Jiangping Hu provided DFT calculations; Fucong Chen, Yangmu Li, and Kui Jin wrote the paper with input from all authors.

Appendix A. Supplementary materials

Supplementary materials to this short communication can be found online at https://doi.org/10.1016/j.scib.2023.03.018.

References

[1] Bardeen J, Cooper LN, Schrieffer JR. Microscopic theory of superconductivity. Phys Rev 1957;106:162–4.
[2] Keimer B, Kivelson SA, Norman MR, et al. From quantum matter to high-temperature superconductivity in copper oxides. Nature 2015;518:179–86.
[3] Cao Y, Fatemi V, Fang S, et al. Unconventional superconductivity in magic-angle graphene superlattices. Nature 2018;556:43.
[4] Ye JT, Zhang YJ, Akashi R, et al. Superconducting dome in a gate-tuned band insulator. Science 2012;338:1193.
[5] Mizuguchi Y, Takano Y. Review of Fe chalcogenides as the simplest Fe-based superconductor. J Phys Soc Jpn 2010;79:102001.
[6] Li D, Lee K, Wang BY, et al. Superconductivity in an infnite-layer nickelate. Nature 2019;572:624–7.
[7] Matthias BT, Hulm JK. A search for new superconducting compounds. Phys Rev 1952;87:799–806.
[8] Tou H, Maniwa Y, Koiwasaki T, et al. Unconventional superconductivity in electron-doped layered $Li_{0.48}(THF)_yHfNCl$. Phys Rev Lett 2001;86:5775.
[9] Kasahara Y, Kuroki K, Yamanaka S, et al. Unconventional superconductivity in electron-doped layered metal nitride halides MNX (M = Ti, Zr, Hf; X = Cl, Br, I). Physica C 2015;514:354–67.
[10] Cooper RA, Wang Y, Vignolle B, et al. Anomalous criticality in the electrical resistivity of $La_{2-x}Sr_xCuO_4$. Science 2009;323:603–7.
[11] Yuan J, Chen Q, Jiang K, et al. Scaling of the strange-metal scattering in unconventional superconductors. Nature 2022;602:431.
[12] Chen XJ, Struzhkin VV, Kung S, et al. Pressure-induced phonon frequency shifts in transition-metal nitrides. Phys Rev B 2004;70:014501.
[13] Ching WY, Xu Y, Ouyang L. Electronic and dielectric properties of insulating Zr_3N_4. Phys Rev B 2022;66:235106.
[14] Badoux S, Tabis W, Laliberté F, et al. Change of carrier density at the pseudogap critical point of a cuprate superconductor. Nature 2016;531:210.
[15] Grissonnanche G, Fang Y, Legros A, et al. Linear-in temperature resistivity from an isotropic Planckian scattering rate. Nature 2021;595:667.

Fucong Chen obtained his B.S. degree in Physics from Beijing Normal University and is a Ph.D. candidate at the Institute of Physics (IOP), Chinese Academy of Sciences (CAS). He studies superconducting films such as $MgTi_2O_4$, FeSe, YBCO, and transition metal nitrides. His current research interest focuses on high-quality superconducting films for technological applications.

Yangmu Li is currently an associate professor at IOP, CAS. He received his Ph.D. degree in Physics at the University of Minnesota in 2017 and worked at Brookhaven National Laboratory before joining IOP in 2021. His research interest includes multi-scale, multi-dimensional spectroscopy measurements of superconductivity and magnetism using quantum sensing techniques.

Kui Jin is the director of National Laboratory for Superconductivity in IOP, CAS. He has been leading a CAS Interdisciplinary Innovation Team on High-throughput Superconductivity Research since 2018, and served as the chief scientist of both the Key Area R&D Program of Guangdong Province (since 2020) and the National Key R&D Program of China (since 2021). His team has been devoted to investigating the mechanism of high-temperature superconductivity and relevant key scientific issues in practical applications.